

## THE DYNAMICAL STRUCTURE OF DARK MATTER HALOS WITH UNIVERSAL PROPERTIES

EMMANUEL VAN HESE, MAARTEN BAES AND HERWIG DEJONGHE  
 Sterrenkundig Observatorium, Universiteit Gent, Krijgslaan 281 S9, B-9000 Gent, Belgium  
*Draft version December 3, 2018*

### ABSTRACT

$N$ -body simulations have unveiled several apparently universal properties of dark matter halos, including a cusped density profile, a power-law pseudo phase-space density  $\rho/\sigma_r^3$ , and a linear  $\beta-\gamma$  relation between the density slope and the velocity anisotropy. We present a family of self-consistent phase-space distribution functions  $F(E, L)$ , based on the Dehnen-McLaughlin Jeans models, that incorporate these universal properties very accurately. These distribution functions, derived using a quadratic programming technique, are analytical, positive and smooth over the entire phase space and are able to generate four-parameter velocity anisotropy profiles  $\beta(r)$  with arbitrary asymptotic values  $\beta_0$  and  $\beta_\infty$ . We discuss the orbital structure of six radially anisotropic systems in detail and argue that, apart from its use for generating initial conditions for  $N$ -body studies, our dynamical modeling provides a valuable complementary approach to understand the processes involved in the formation of dark matter halos.

*Subject headings:* cosmology: dark matter – galaxies: clusters: general – galaxies: kinematics and dynamics – methods: analytical

### 1. INTRODUCTION

In theoretical astrophysics the steady increase in computational power has sparked a proportional interest and progress in the study of large-scale structure formation. In particular, as  $N$ -body simulations of cold dark matter halos have become more detailed, several "universal" properties have emerged. We highlight three important characteristics.

Firstly, numerous cosmological studies (e.g. Dubinski & Carlberg 1991; Crone et al. 1994; Navarro et al. 1996; Fukushige & Makino 1997; Navarro et al. 1997; Carlberg et al. 1997; Moore et al. 1998, 1999; Jing & Suto 2000) revealed similar density profiles over several orders of magnitude in halo mass, with a central cusp and an  $\rho(r) \propto r^{-3}$  falloff at large radii. These generalized NFW models can be described by a general 3-parameter family, referred to as the Zhao models (or  $\alpha\beta\gamma$ -models) (Hernquist 1990; Zhao 1996). They are defined by the density

$$\rho(r) = \frac{2^{(\gamma_\infty - \gamma_0)/\eta} \rho_s}{(r/r_s)^{\gamma_0} (1 + (r/r_s)^\eta)^{(\gamma_\infty - \gamma_0)/\eta}}, \quad (1)$$

or in terms of the logarithmic slope,

$$\gamma(r) = -\frac{d \ln \rho}{d \ln r}(r) = \frac{\gamma_0 + \gamma_\infty (r/r_s)^\eta}{1 + (r/r_s)^\eta}. \quad (2)$$

Although in recent years alternative profiles based on the Sérsic law have produced equally good results (Navarro et al. 2004; Merritt et al. 2005), the generalized NFW models remain very popular and successful to represent dark matter halos.

A second relation was found by Taylor & Navarro (2001). These authors identified that the quantity  $Q(r) = \rho/\sigma_r^3(r)$ , which has become known as the pseudo phase-space density, behaves as a power law over 2-3 orders of magnitude in radius

inside the virial radius,

$$Q(r) \propto r^{-\alpha}. \quad (3)$$

Other studies (e.g. Rasia et al. 2004; Ascasibar et al. 2004) have confirmed the scale-free nature of  $Q(r)$ , and their results indicate that its slope lies in the range  $\alpha = 1.90 \pm 0.05$ . This property is remarkable since the density  $\rho(r)$  nor the velocity dispersion  $\sigma(r)$  separately show a power-law behavior.

Finally, the velocity anisotropy profiles  $\beta(r)$  of dark matter systems also evolve toward a similar shape, steepening gradually from isotropic in the center to radially anisotropic in the outer regions. Hansen & Moore (2006) suggest a nearly linear relation between the logarithmic density slope  $\gamma(r)$  and the velocity anisotropy profile, based on various types of equilibrated simulations. They proposed the  $\beta-\gamma$  relation

$$\beta(\gamma) \simeq 1 - 1.15(1 + \gamma/6). \quad (4)$$

Several theoretical studies have been made to investigate whether solutions of the Jeans equation exist that encompass the observed properties of dark matter halos. In particular, Dehnen & McLaughlin (2005) investigated the anisotropic Jeans equation constrained by a slightly different form of the pseudo phase-space density, namely  $Q_r(r) = \rho/\sigma_r^3$  with  $\sigma_r(r)$  the radial velocity dispersion. They found a special solution, namely an analytical self-consistent potential-density pair of the form (1) with an anisotropy profile

$$\beta(r) = \frac{\beta_0 + \beta_\infty (r/r_a)^{2\delta}}{1 + (r/r_a)^{2\delta}}, \quad (5)$$

that also has an exactly linear  $\beta-\gamma$  relation (in other words,  $r_a = r_s$  and  $2\delta = \eta$ ). As these Jeans models satisfy the three universal relations mentioned above, we can consider them as representative models for realistic dark matter halos.

The goal of this paper is to take the analytical study of dark matter systems a step further, i.e. to look for full dynamical models that encompass the universal properties found in  $N$ -body simulations. In concreto we will look for phase-space distribution functions (DFs)  $F(\vec{r}, \vec{v})$  that self-consistently generate the required density, potential, and anisotropy profiles

Electronic address: emmanuel@heze.ugent.be  
 Electronic address: maarten.baes@ugent.be  
 Electronic address: herwig.dejonghe@ugent.be

encountered in dark matter halos. Such dynamical models would provide a very useful complementary approach to gain insight into the structure of dark matter halos.

We shall focus on spherical models, for which a dynamical description simplifies substantially as in this case the DF can be expressed as a function  $F(E, L)$  of the binding energy and the angular momentum. But even if we limit ourselves to the spherical case, it is not straightforward to obtain such dynamical models. A simple approach is to solve the Jeans equation and approximate the velocity dispersion profiles by a multivariate Gaussian (Hernquist 1993). Kazantzidis et al. (2004) demonstrated however that these systems are far from equilibrium, thus losing their initial dynamical structure as they evolve to non-Gaussian velocity distributions in subsequent  $N$ -body simulations. We therefore need the tools to derive full self-consistent equilibrium models, governed by DFs with a sufficiently general velocity anisotropy profile.

Simple analytical models are found for only a few special cases, such as the Plummer, Hernquist, isochrone, and  $\gamma$ -models (e.g. Dejonghe 1987; Hernquist 1990; Baes & Dejonghe 2002; An & Evans 2006; Buyle et al. 2007a), none of which are able to describe realistic dark matter halos. For general potential-density pairs, Osipkov (1979) and Merritt (1985) provided an algorithm to construct dynamical models with a specific velocity anisotropy profile of the form (5), with  $\beta_0 = 0$ ,  $\beta_\infty = 1$  and  $\delta = 1$ , leaving  $r_a$  as a free parameter. While the Osipkov-Merritt method has been widely adopted (e.g. Widrow 2000; Łokas & Mamon 2001; Kazantzidis et al. 2004), comparison with simulations shows that such anisotropy profiles are too steep to describe dark matter (Mamon & Łokas 2005). Halos are not completely radial at infinity (i.e.  $\beta_\infty < 1$ ) and the linear  $\beta - \gamma$  relation can only be realized with a lower transition rate  $\delta < 1$ . On a dynamical note, the associated DFs are of the form  $F(Q)$  with  $Q = E - L^2/2r_a^2$ , creating an unphysical cut-off boundary for orbits with  $Q < 0$ . Hence, the Osipkov-Merritt framework is too limited to generate realistic dark matter systems, and a more extensive method is needed.

Recently, Wojtak et al. (2008) presented an interesting approach to generate dynamical models for potential-density pairs with a more general anisotropy profile. They proposed to express the DF as a separable function of the form  $f_E(E)f_L(L)$  where  $f_L(L)$  is a double power-law function with three parameters  $\beta_0$ ,  $\beta_\infty$ , and  $L_0$ . Once their values have been determined, the function  $f_E(E)$  is derived from the observed density profile by a numerical inversion. This technique yields a three-parameter anisotropy profile that resembles eq. (5), where  $L_0$  has a similar role as  $r_a$ , and a fixed transition rate  $0.5 < \delta < 1$ . In this manner, the authors were able to construct models with an NFW density with velocity dispersion profiles that agreed with their dark matter simulations.

In this paper, we present a technique that enables us to obtain dynamical models with exactly the four-parameter anisotropy profile (5). We demonstrated in a previous paper (Baes & Van Hese 2007, hereafter Paper I) how this can be achieved, by postulating a separable parameterized form of the so-called augmented density, which provides an equivalent description of a dynamical system. In certain special cases the transformation from the augmented density to the DF is analytically tractable. We were thus able to derive a family of DFs for the generalized Plummer models (also called  $\alpha$ -models or Veltmann models, Veltmann (1979)) with a linear  $\beta - \gamma$  relation.

Since the generalized Plummer potential-density pairs form a special class of the Zhao models (1), we will now demonstrate that this result is a first step toward more representative dark matter profiles. In particular, we seek a family of DFs for the Dehnen-McLaughlin systems, because of their unique property to satisfy a universal density, a power law  $Q_r(r)$ , and a linear  $\beta - \gamma$  relation. We use a quadratic programming technique (Dejonghe 1989) to build DFs as a linear combination of base functions of the form derived in Paper I. In this manner, we demonstrate that it is indeed possible to generate full dynamical models for the Dehnen-McLaughlin Jeans models, thus providing DFs that encompass the observed properties of dark matter halos.

Our paper is organized as follows. In Section 2 we describe the notion of a dynamical model and we briefly summarize the main aspects of the Dehnen-McLaughlin halos. Next we outline our modeling technique in Section 3: we explain the quadratic programming algorithm and we recapitulate the functions that we derived in Paper I. With these components, we can build a library to apply the QP-method to the Dehnen-McLaughlin halos. In Section 4 we present our results for a set of systems with different velocity anisotropy profiles, and we discuss the moments, phase-space DFs, and energy and angular momentum distributions for these models. Finally, we formulate our conclusions in Section 5.

## 2. PRELIMINARIES

### 2.1. Dynamical models

The dynamical structure of a gravitational equilibrium system is completely determined by the DF  $F(\vec{r}, \vec{v})$ , which describes the probability distribution of particles in six-dimensional phase space. A dynamical model is only physical if its DF is non-negative everywhere. In the case of spherical symmetry, this DF can be written as a function  $F(E, L)$  of two isolating integrals, namely the binding energy and the angular momentum

$$E = \psi(r) - \frac{1}{2}v_r^2 - \frac{1}{2}v_T^2, \quad (6)$$

$$L = r v_T, \quad (7)$$

with

$$v_T = \sqrt{v_\theta^2 + v_\phi^2}, \quad (8)$$

the transverse velocity, and  $\psi(r)$  the positive binding potential. For circular orbits the integrals of motion can be written in function of the radius  $r$ ,

$$E_c(r) = \psi(r) + \frac{r}{2} \frac{d\psi}{dr}(r), \quad (9)$$

$$L_c(r) = -r^3 \frac{d\psi}{dr}(r), \quad (10)$$

which can be solved to obtain  $E_c(L)$  and  $L_c(E)$ . All dynamical properties can be derived from the DF, such as the anisotropic velocity moments

$$\mu_{2n, 2m}(r) = 2\pi M_{\text{tot}} \int_{-\infty}^{+\infty} dv_r \int_0^{+\infty} F(E, L) v_r^{2n} v_T^{2m+1} dv_T, \quad (11)$$

with  $M_{\text{tot}}$  the total mass. If the system is self-consistent, then the density  $\rho(r) = \mu_{00}(r)$  is connected to the potential via the Poisson equation

$$\frac{1}{r^2} \frac{d}{dr} \left( r^2 \frac{d\psi}{dr} \right) (r) = -4\pi G \rho(r). \quad (12)$$

Furthermore, the second-order moments determine the radial and tangential velocity dispersions  $\mu_{20}(r) = \rho\sigma_r^2(r)$  and  $\mu_{02}(r) = 2\rho\sigma_\theta^2(r)$ , and the velocity anisotropy profile

$$\beta(r) = 1 - \frac{\sigma_\theta^2(r)}{\sigma_r^2(r)}. \quad (13)$$

A DF is only fully determined when all velocity moments (11) are known (Dejonghe 1987). However, it is already far from trivial to obtain *any* non-negative DF that adequately generates a given density  $\rho(r)$  and anisotropy profile  $\beta(r)$ . In this paper, we will focus our attention to one specific family of halos, namely the Dehnen-McLaughlin Jeans models, and we demonstrate that a family of DFs can indeed be constructed for these systems.

### 2.2. The Dehnen-McLaughlin halos

In the context of theoretical dark matter studies, the model derived by Dehnen & McLaughlin (2005) is of particular interest. We summarize their main results in this section. Instead of fitting a parameterized density profile to  $N$ -body simulations, they investigated the solution space of the Jeans equation to search for models that explicitly obey the power-law behavior of the pseudo phase-space density. With the extra condition of a linear  $\beta - \gamma$  relation they found a critical solution that satisfies the condition

$$\frac{\rho}{\sigma_r^\varepsilon}(r) = \frac{\rho}{\sigma_r^\varepsilon}(r_s) \left(\frac{r}{r_s}\right)^{-\alpha_{\text{crit}}}, \quad (14)$$

with  $r_s$  a scale radius. In the remainder of this paper, we adopt the common value  $\varepsilon = 3$  and use the notation  $Q_r(r) = \rho/\sigma_r^3$ . Dehnen & McLaughlin derived for this case the exponent

$$\alpha_{\text{crit}} = \eta + \frac{3}{2}, \quad (15)$$

$$\eta = \frac{4 - 2\beta_0}{9}, \quad (16)$$

with  $\beta_0$  the central velocity anisotropy. The corresponding potential-density pair is fully analytical, given by

$$\psi(r) = \frac{GM_{\text{tot}}}{r_s} \frac{1}{\eta} B_{\frac{1}{1+x^\eta}} \left( \frac{1}{\eta}, \frac{1-\beta_0}{\eta} + \frac{1}{2} \right), \quad (17)$$

$$\rho(r) = \frac{4 + \eta - 2\beta_0}{8\pi} \frac{M_{\text{tot}}}{r_s^3} x^{-\gamma_0} (1+x^\eta)^{-(\gamma_\infty - \gamma_0)/\eta}, \quad (18)$$

where  $x = r/r_s$ ,  $B_y(a, b)$  is the incomplete beta function and

$$\gamma_0 = \frac{7 + 10\beta_0}{9}, \quad (19)$$

$$\gamma_\infty = \frac{31 - 2\beta_0}{9}. \quad (20)$$

The density can be equivalently written in terms of the slope  $\gamma(r)$ , which has the same elegant form as the velocity anisotropy profile  $\beta(r)$

$$\gamma(r) = \frac{\gamma_0 + \gamma_\infty x^\eta}{1 + x^\eta}, \quad (21)$$

$$\beta(r) = \frac{\beta_0 + \beta_\infty x^\eta}{1 + x^\eta}. \quad (22)$$

Finally, the authors derived the corresponding velocity dispersions

$$\sigma_r^2(r) = \frac{1}{4 + \eta - 2\beta_\infty} \frac{GM_{\text{tot}}}{r_s} x^{-1} \left( \frac{x^\eta}{1 + x^\eta} \right)^{(\gamma_\infty - \gamma_0)/\eta - 2}, \quad (23)$$

$$\sigma_\theta^2(r) = \sigma_\varphi^2(r) = \frac{1}{2} \sigma_T^2(r) = (1 - \beta(r)) \sigma_r^2(r). \quad (24)$$

Eqs. (14)-(24) characterize the Dehnen-McLaughlin models; we refer to their paper for more details. These systems are determined by five parameters: the exponent  $\varepsilon$  in the pseudo phase-space density, two scaling constants i.e. the total mass  $M_{\text{tot}}$  and the scale radius  $r_s$ , and the asymptotic anisotropy parameters  $\beta_0$  and  $\beta_\infty$ . The authors also noted the remarkable property that the shape of the density profile (and hence the gravitational potential) only depends on  $\beta_0$  and not on  $\beta_\infty$ .

While the Dehnen-McLaughlin Jeans models are derived from theoretical considerations, they also fit adequately galaxy-sized and certain cluster-sized halos generated by  $N$ -body simulations (Diemand et al. 2005; Merritt et al. 2006). But as mentioned in the previous Section, the density and velocity dispersions alone do not determine the complete dynamical state of dark matter systems. We therefore aim to incorporate these profiles into self-consistent dynamical models, described by non-negative DFs.

### 3. THE MODELING TECHNIQUE

To find DFs that describe the Dehnen-McLaughlin Jeans models, we adopt the mathematical framework that we derived in Paper I. These tools enabled us to construct a family of components with the anisotropy profile (5), by means of the powerful augmented density concept. We summarize these results, and we demonstrate how to build a linear combination of these components using a quadratic programming (QP) technique (Dejonghe 1989). In this manner, we can fit a dynamical model to a given halo.

#### 3.1. The augmented density concept

Since our dynamical models have to reproduce the moments (18), (23) and (24), we first seek DFs that are specifically designed for this task. This can be done by introducing the augmented densities  $\tilde{\rho}(\psi, r)$  (Dejonghe 1986), which extend the densities to explicit functions of both the radius and the gravitational potential. Like the DF, the augmented density uniquely determines the dynamical state of a spherical equilibrium system. Both functions are connected by the relation

$$\tilde{\rho}(\psi, r) = 2\pi M_{\text{tot}} \int_0^\psi dE \int_0^{2(\psi-E)} \frac{F(E, r v_T)}{\sqrt{2(\psi-E) - v_T^2}} dv_T^2. \quad (25)$$

If we define that all functions are zero when their arguments lie outside their physical bounds, we can use the Laplace-Mellin transforms

$$\mathcal{L}_{E \rightarrow \xi} \mathcal{M}_{L \rightarrow \lambda} \{F\} = \int_0^{+\infty} e^{-\xi E} dE \int_0^{+\infty} L^{\lambda-1} F(E, L) dL, \quad (26)$$

$$\mathcal{L}_{\psi \rightarrow \xi} \mathcal{M}_{r \rightarrow \lambda} \{\tilde{\rho}\} = \int_0^{+\infty} e^{-\xi \psi} d\psi \int_0^{+\infty} r^{\lambda-1} \tilde{\rho}(\psi, r) dr, \quad (27)$$

with the inverse transforms

$$F(E, L) = \frac{-1}{4\pi^2} \int_{\xi_0 - i\infty}^{\xi_0 + i\infty} e^{\xi E} d\xi \int_{\lambda_0 - i\infty}^{\lambda_0 + i\infty} L^{-\lambda} \mathcal{L}_{E \rightarrow \xi} \mathcal{M}_{L \rightarrow \lambda} \{F\} dL, \quad (28)$$

$$\tilde{\rho}(\psi, r) = \frac{-1}{4\pi^2} \int_{\xi_0 - i\infty}^{\xi_0 + i\infty} e^{\xi \psi} d\xi \int_{\lambda_0 - i\infty}^{\lambda_0 + i\infty} r^{-\lambda} \mathcal{L}_{\psi \rightarrow \xi} \mathcal{M}_{r \rightarrow \lambda} \{\tilde{\rho}\} dr. \quad (29)$$

Combining these expressions with (25), we obtain

$$\mathcal{L}_{\psi \rightarrow \xi} \mathcal{M}_{r \rightarrow \lambda} \{\tilde{\rho}\} = 2\pi M_{\text{tot}} \int_0^{+\infty} e^{-\xi \psi} d\psi \int_0^{+\infty} v_T^{-\lambda} L^{\lambda-1} dL$$

$$\times \int_0^\psi dE \int_0^{2(\psi-E)} \frac{F(E, L) dv_T^2}{\sqrt{2(\psi-E)-v_T^2}}. \quad (30)$$

Interchanging the integrals yields the formal relation

$$\mathcal{L}_{E \rightarrow \xi} \mathcal{M}_{L \rightarrow \lambda} \{F\} = \frac{2^{\lambda/2}}{M_{\text{tot}}(2\pi)^{3/2}} \frac{\xi^{(3-\lambda)/2}}{\Gamma(1-\frac{\lambda}{2})} \mathcal{L}_{\psi \rightarrow \xi} \mathcal{M}_{r \rightarrow \lambda} \{\tilde{\rho}\}. \quad (31)$$

The main strength of the augmented density formalism is the ability to impose very specific conditions on these functions, to obtain our objective. More precisely, we demonstrated in Paper I that separable functions of the form

$$\tilde{\rho}(\psi, r) = f(\psi)g(r), \quad (32)$$

are particularly interesting, since in this case  $g(r)$  is directly related to the velocity anisotropy profile,

$$\beta(r) = -\frac{1}{2} \frac{d \ln g}{d \ln r}(r). \quad (33)$$

With this formalism it is therefore at least formally possible to generate a DF for a dynamical system with a given potential  $\psi(r)$ , density  $\rho(r)$ , and velocity anisotropy profile  $\beta(r)$ . If we postulate an anisotropy profile of the form (5), the modeling procedure reduces to the computation of  $f(\psi)$  such that

$$\rho(r) = f(\psi(r)) \left(\frac{r}{r_a}\right)^{-2\beta_0} \left(1 + \frac{r^{2\delta}}{r_a^{2\delta}}\right)^{\beta_\delta}, \quad (34)$$

with  $0 < \delta \leq 1$  and

$$\beta_\delta = \frac{\beta_0 - \beta_\infty}{\delta}. \quad (35)$$

Evidently, the exact solution  $f(\psi)$  is generally of numerical form, except for a few special cases. This creates a problem to recover the DF from the augmented density, because a direct inversion of the Laplace-Mellin transformation in (31) is in general numerically unstable (Dejonghe 1986). Indeed, the double integration in (25) smooths features in  $F(E, L)$  and the inversion procedure of determining  $F(E, L)$  from  $\tilde{\rho}(\psi, r)$  has the delicate job of unsmoothing the information contained in  $\tilde{\rho}(\psi, r)$ . Consequently, a direct inversion can only be performed safely for sufficiently simple forms of  $f(\psi)$ .

We therefore take an alternative approach. Instead of solving (34) directly, we will approximate the given density profile by a linear combination of simple base functions  $\tilde{\rho}_i(\psi(r), r)$  for which the Laplace-Mellin inversions are analytical. The corresponding DF is then simply the same linear combination of the associated base DFs  $F_i(E, L)$ , resulting in an analytically tractable function. This can be achieved by a least squares fit to a set of density data points, defining a quadratic programming problem in the unknown coefficients. Various authors have successfully used a similar modeling technique (Kuijken & Merrifield 1993; Merrifield & Kuijken 1994; Gerhard et al. 1998). A QP-algorithm, suited for this task, has been developed in our department (Dejonghe 1989), which we outline in the following Section.

### 3.2. The quadratic programming procedure

Consider a given potential  $\psi(r)$ , an anisotropy profile  $\beta(r)$  of the form (5) and a set of  $M$  density data points  $\rho_{\text{obs}}(r_m)$ ,  $m = 1, \dots, M$ . To model these data, we first construct a library of  $N_{\text{lib}}$  base functions

$$\tilde{\rho}_i(\psi, r) = f_i(\psi) \left(\frac{r}{r_a}\right)^{-2\beta_0} \left(1 + \frac{r^{2\delta}}{r_a^{2\delta}}\right)^{\beta_\delta}, \quad (36)$$

with  $f_i(\psi)$  sufficiently simple to compute the associated distributions  $F_i(E, L)$ . From these components, we can extract the corresponding values

$$\rho_i(r_m) = \tilde{\rho}_i(\psi(r_m), r_m), \quad m = 1, \dots, M. \quad (37)$$

Our aim is now to construct a linear combination of  $N$  components from this library that provides an adequate fit to the given data. Such a fit can be obtained in a statistically meaningful way by minimizing the quantity

$$\chi_N^2 = \frac{1}{M} \sum_{m=1}^M w_m \left( \rho_{\text{obs}}(r_m) - \sum_{i=1}^N a_{N,i} \rho_i(r_m) \right)^2, \quad (38)$$

which is a quadratic function of the coefficients  $a_{N,i}$ , consequently defining a quadratic programming problem. The data points are given equal weights by setting the constants  $w_m = 1/\rho_{\text{obs}}^2(r_m)$ .

To find such a set, we use an iterative algorithm (Dejonghe 1989). With this method, a set of components is successively built in  $N$  steps. In the first step,  $N_{\text{lib}}$   $\chi^2$ -minimizations are performed using in turn each component of the library. The base function that yields the lowest  $\chi^2$ -value (hereafter denoted  $\chi_1^2$ ) is retained as the first element of our best-fitting set, with corresponding coefficient  $a_{1,1}$ . In each next iteration, the functions in this set are preserved, while the coefficients are allowed to vary. The set is subsequently extended by adding the component from the library that yields the most improvement of the fit, minimizing over all coefficients. In other words, suppose we have obtained the best-fitting set of  $N-1$  base functions, with indices  $n_1, \dots, n_{N-1}$ . Then, we add in turn the remaining  $N_{\text{lib}} - N + 1$  components from the library, and calculate the  $N$  coefficients for each combination by means of the  $\chi^2$ -minimizations

$$\chi_{(n_N)}^2 = \min_{a_1, \dots, a_N} \frac{1}{M} \sum_{m=1}^M w_m \left( \rho_{\text{obs}}(r_m) - \sum_{i=1}^N a_i \rho_{n_i}(r_m) \right)^2, \quad (39)$$

with  $n_N \in \{1, \dots, N_{\text{lib}}\} \setminus \{n_1, \dots, n_{N-1}\}$ .

From these  $N_{\text{lib}} - N + 1$  values, we determine the best fit

$$\chi_N^2 = \chi_{(n_{\text{min}})}^2 = \min_{n_N} \chi_{(n_N)}^2, \quad (40)$$

and add the base function with index  $n_{\text{min}}$  to the best-fitting set, denoting  $n_N = n_{\text{min}}$ . By renaming the indices of this set, we thus obtain a linear combination of  $N$  base functions  $\tilde{\rho}_i(\psi, r)$  with coefficients  $a_{N,i}$  and a goodness of fit  $\chi_N^2$ . The corresponding DF is then simply

$$F(E, L) = \sum_{i=1}^N a_{N,i} F_i(E, L). \quad (41)$$

The QP-algorithm allows additional linear constraints on the coefficients. In particular, we impose upper and lower boundaries

$$a_{\text{min}} \leq a_{N,i} \leq a_{\text{max}}, \quad \forall N; i = 1, \dots, N. \quad (42)$$

These constraints are not necessary, but they greatly reduce the computational cost in the calculation of the DF. The reason for this is straightforward: if the components are computed with numerical errors  $\delta_i F_i$  then the total numerical error of the DF is

$$\delta F(E, L) = \frac{\sum_{i=1}^N |a_{N,i}| \delta_i F_i(E, L)}{\sum_{i=1}^N a_{N,i}}. \quad (43)$$

The higher the absolute values of the coefficients  $|a|_{N,i}$ , the smaller the errors  $\delta_i F_i$  need to be to obtain a given  $\delta F$ , which increases the computational time. Sensible boundary values (42) enable efficient calculations of the DF, while maintaining satisfactory fits.

The resulting DF also needs to be physical, i.e. non-negative everywhere in phase space. We found that all our DFs automatically satisfy this condition without imposing explicit constraints.

This procedure has several advantages. The resulting DF remains analytically tractable, which also simplifies the computation of all the moments of this dynamical model. Furthermore, only a limited number of data points are required, rather than the entire density profile. The same algorithm can also be applied to data extracted from simulations or observations, and a variety of different moments besides the density can be used in the fitting procedure.

Finally, since all components have a priori the desired  $\beta(r)$ , their linear combination will automatically generate the same anisotropy profile. This is a very significant benefit. Indeed, practice has shown that it is particularly difficult to construct radially anisotropic systems from base functions that are too simple (such as Fricke components, Fricke (1952)) with different constant anisotropies. In that case an additional fitting is required to the second-order moments. But more importantly, because radial orbits influence the density both at small and large radii, the summation of components with different anisotropies results into a delicate fine-tuning to obtain adequate fits to both the density and the velocity anisotropy. These problems are avoided if the components already have the correct anisotropy profile, and although it is more intricate to design such functions, this approach greatly reduces the complexity of the quadratic programming procedure.

### 3.3. The base functions

We are now left with the construction of a library of adequate base functions  $\tilde{\rho}_i(\psi, r)$ . The success of our modeling is largely determined by this library. As stated above, the components have to generate the anisotropy profile (5), while being sufficiently simple to retrieve the corresponding DFs  $F_i(E, L)$  from eq. (31). In addition, the subsequent densities  $\rho_i(r_m)$  need to be able to reproduce the specific characteristics of the given data to obtain a satisfactory fit. In the particular case of the Dehnen-McLaughlin halos (18), this implies that the components should incorporate the central density cusp and the asymptotic density slope at large radii, using the given potential (17). In Paper I we derived a family of base functions that meet all these requirements. Consider the family of augmented densities

$$\tilde{\rho}_i(\psi, r) = \rho_{0i} \left( \frac{\psi}{\psi_0} \right)^{p_i} \left( 1 - \frac{\psi^{s_i}}{\psi_0^{s_i}} \right)^{q_i} \left( \frac{r}{r_a} \right)^{-2\beta_0} \left( 1 + \frac{r^{2\delta}}{r_a^{2\delta}} \right)^{\beta_\delta}, \quad (44)$$

where  $\rho_{0i}$  are normalization constants such that

$$4\pi \int_0^{+\infty} \tilde{\rho}_i(\psi(r), r) r^2 dr = 1, \quad (45)$$

and  $\psi_0$  denotes the depth of the (finite) potential well,  $\psi_0 = \psi(0)$ . The normalization constants are chosen such that the sum of the coefficients of a good fit should approximate the total mass of the input data, i.e.  $\sum_{i=1}^N a_{N,i} \simeq M_{\text{tot}}$ .

Apart from the four fixed parameters that determine the anisotropy profile (22), the  $f(\psi)$ -part of these functions con-

tains three additional free parameters  $p_i$ ,  $q_i$  and  $s_i$ , which respectively determine the asymptotic behavior at infinity, the inner slope, and the transition rate between these two regions. They satisfy the conditions  $p_i + 2\beta_\infty > 3$ ,  $q_i \leq 0$  and  $s_i > 0$ .

All other dynamical properties can be calculated from these augmented densities. The augmented higher-order moments are derived in Appendix A, and we demonstrated in the Appendices of Paper I that for these  $\rho_i(\psi, r)$  the inverse Laplace-Mellin transforms can be performed analytically in eq. (31). The corresponding distribution functions can be expressed as a series of Fox  $H$ -functions (Fox 1961):

$$F_i(E, L) = \frac{\rho_{0i}}{M_{\text{tot}}(2\pi\psi_0)^{3/2}} \times \sum_{j=0}^{\infty} (-1)^j \binom{q_i}{j} \frac{\Gamma(1+p_i+js_i)}{\delta\Gamma(-\beta_\delta)} \left( \frac{E}{\psi_0} \right)^{p_i+js_i-3/2} \times H_{2,2}^{1,1} \left( \frac{L^2}{2r_a^2 E} \left| \begin{array}{c} \left( 1 - \frac{\beta_\infty}{\delta}, \frac{1}{\delta} \right), \left( p_i + js_i - \frac{1}{2}, 1 \right) \\ \left( -\frac{\beta_0}{\delta}, \frac{1}{\delta} \right), (0, 1) \end{array} \right. \right), \quad (46)$$

which can be written as a double series

$$F_i(E, L) = \frac{\rho_{0i}}{M_{\text{tot}}(2\pi\psi_0)^{3/2}} \sum_{j=0}^{\infty} (-1)^j \binom{q_i}{j} \left( \frac{E}{\psi_0} \right)^{p_i+js_i-3/2} \times \sum_{k=0}^{\infty} \binom{\beta_\delta}{k} \frac{\Gamma(1+p_i+js_i)}{\Gamma(p_i+js_i-\frac{1}{2}+\beta_k)\Gamma(1-\beta_k)} \left( \frac{L^2}{2r_a^2 E} \right)^{-\beta_k} \quad (47)$$

where we used the auxiliary notation

$$\beta_k = \begin{cases} \beta_0 - k\delta & \text{for } L^2 < 2r_a^2 E, \\ \beta_\infty + k\delta & \text{for } L^2 > 2r_a^2 E. \end{cases} \quad (48)$$

The double summation  $\sum_j \sum_k$  can be computed by changing the indices to  $\sum_l \sum_{j+k=l}$ , so that the inner summation becomes a finite sum of  $l+1$  terms for each value of  $l$ ; the index  $l$  is increased until the total sum alters by less than a required numerical error  $\delta_i F_i$ . Due to the double summation, the computational time is an inverse quadratic function of  $\delta_i F_i$ .

We proved in Paper I that these base DFs are continuous and non-negative everywhere in physical phase space. Moreover, we showed that they generate exactly the generalized Plummer potential-density pairs (Veltmann 1979)

$$\psi_{\text{gp}}(r) = \frac{GM_{\text{tot}}}{(r_s^\eta + r^\eta)^{1/\eta}}, \quad (49)$$

$$\rho_{\text{gp}}(r) = \frac{(1+\eta)M_{\text{tot}}}{4\pi} \frac{r_s^\eta}{r^{2-\eta}(r_s^\eta + r^\eta)^{2+1/\eta}}, \quad (50)$$

with a linear  $\beta-\gamma$  relation. Since these systems are closely related to the Dehnen-McLaughlin halos, this is a promising result for the success of the quadratic programming routine.

The FORTRAN source code with the DF base functions and the augmented moments is available on request.

### 3.4. The library of components

Every given Dehnen-McLaughlin halo requires a specific component library. In particular, the parameters  $p_i$ ,  $q_i$  are constrained by the potential. If we examine the asymptotic behavior of the Dehnen-McLaughlin potential (17) in more

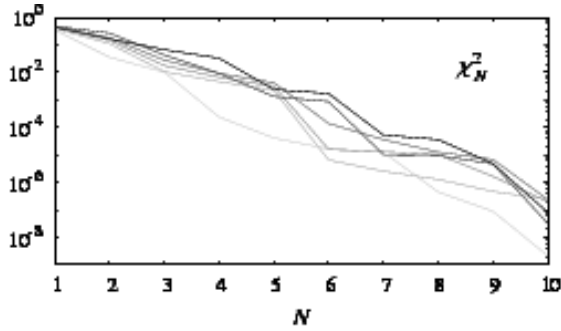


FIG. 1.— The obtained  $\chi_N^2$  for the six QP-models, explicitly as a function of the number of components in the fit. The different curves correspond to  $\beta_\infty = 0, 0.2, 0.4, 0.6, 0.8$  and  $1$ , with a grayscale ranging from black ( $\beta_\infty = 0$ ) to lightgray ( $\beta_\infty = 1$ ). In detail, we find

$$\begin{aligned} \psi(r) &\sim \psi_0 - ar^{(11-10\beta_0)/9} + \dots \quad \text{for } r \rightarrow 0, \\ \psi(r) &\sim \frac{1}{r} \quad \text{for } r \rightarrow \infty. \end{aligned} \quad (51)$$

Introducing these asymptotic expansions in the expression (44) we find for the inner and outer slopes of the density

$$\begin{aligned} \tilde{\rho}_i(\psi(r), r) &\sim r^{-2\beta_0 + q_i(11-10\beta_0)/9} \quad \text{for } r \rightarrow 0, \\ \tilde{\rho}_i(\psi(r), r) &\sim r^{-2\beta_\infty - p_i} \quad \text{for } r \rightarrow \infty. \end{aligned} \quad (52)$$

Evidently, the parameters  $p_i$  stipulate the density slope at large radii. Because the models fall as  $r^{-\gamma_\infty}$ , no components can be used in the fitting routine that fall less rapidly. Using eq. (20), this puts a boundary on the  $p_i$ ,

$$p_i \geq \frac{31 - 2\beta_0 - 18\beta_\infty}{9} \equiv p_{\min}(\beta_0, \beta_\infty). \quad (53)$$

Conversely, the density slope at small radii depends on the parameters  $q_i$ . The density diverges toward the center as  $r^{-\gamma_0}$ , and we cannot use components in the fitting routine that have a steeper slope. Thus we obtain from eq. (20)

$$q_i \geq -\frac{7 - 8\beta_0}{11 - 10\beta_0} \equiv q_{\min}(\beta_0). \quad (54)$$

So if a fit to a halo has at least one component with parameter  $p_{\min}$  and one with  $q_{\min}$ , this fit has the same slope as the given density at small and large radii.

Finally, the parameters  $s_i$  have a similar role as  $\delta$ , in the sense that they control the transition rate between the inner and outer density slopes. Their value can be chosen freely, but we found that excellent results are obtained with a single fixed value

$$s_i \equiv 2\delta = \eta, \quad (55)$$

for all components. This is the same choice as the generalized Plummer models in Paper I. It also simplifies the computation of the DFs (47)-(48), and it further facilitates the fitting process, leaving only  $p_i$  and  $q_i$  as free parameters.

## 4. RESULTS

### 4.1. The minimization

Now that we have derived the necessary mathematical tools, we can present the results for the Dehnen-McLaughlin halos. Without loss of generality, we can work in dimensionless units  $G = M_{\text{tot}} = r_s = r_a = 1$ , and we limit ourselves to  $\varepsilon = 3$ . Consequently, the models are determined by the anisotropy parameters  $\beta_0$  and  $\beta_\infty$ . Although we are able to generate models with arbitrary values for these parameters, realistic dark

matter halos are nearly isotropic near the center and radially anisotropic at large radii, so that we concentrate on six representative models with  $\beta_0 = 0$  and  $\beta_\infty = 0, 0.2, 0.4, 0.6, 0.8, 1$ . We verified that the modeling procedure works equally well for models with non-zero values of  $\beta_0$ . Finally, it is evident from eq. (16) that  $\beta_0 = 0$  sets the parameters  $s_i \equiv 2\delta = \eta = 4/9$ .

As we demonstrated above, the very specific form of the base functions (44) simplifies our QP-algorithm considerably for these models. Only the parameters  $p_i$  and  $q_i$  remain to construct a library of components, and we have found that only 30 components are sufficient to yield excellent fits. The parameters  $p_i$  take five values, ranging from  $p_{\min}(0, \beta_\infty)$  to 10 or 12, depending on the model. The parameters  $q_i$  take six values from  $q_{\min}(0)$  to 0. We list these values for each model in the headers of Table 1.

We extract  $M = 25$  values of the density (18) at radii  $r_m$ , distributed logarithmically between  $10^{-3} r_s$  and  $10^4 r_s$ , that serve as input data  $\rho_{\text{obs}}(r_m)$  in each QP-procedure. Evidently, this range is much larger than the virialized region in  $N$ -body simulations. This larger range is therefore not intended to be realistic, but rather to demonstrate that our models are accurate to arbitrary distances. Furthermore, this makes it possible to create discrete equilibrium systems from the DFs, by means of Monte Carlo simulators, that trace very closely the Dehnen-McLaughlin halos. After calculating the densities (44) of every library component at these radii  $\tilde{\rho}_i(\psi(r_m), r_m)$ , we can perform the QP-algorithm for the six values of  $\beta_\infty$ , constructing iteratively the best-fitting linear combination (38) of  $N$  components with additional constraints of the form (42),

$$-100 \leq a_{N,i} \leq 100, \quad \forall N; i = 1, \dots, N. \quad (56)$$

We show the results for the six models in Table 1. The columns list the components of the fits. Every  $\chi_N^2$  denotes the goodness of fit of the best linear combination of the components in columns 1 to  $N$ . Each component is determined by the parameters  $p_i$ , and  $q_i$ , which in turn define the normalization constants  $\rho_{0i}$  from eq. (45). The coefficients are only given for the final fit with 10 components, i.e.  $a_{10,i}$ . It can be checked that for each model

$$\sum_{i=1}^{10} a_{10,i} \simeq M_{\text{tot}} = 1, \quad (57)$$

indicating excellent fits. Combining this result with eqs. (43) and (56), it can be seen that if  $N = 10$ , the numerical errors of the base functions  $\delta_i F_i$  need at most be a factor  $10^3$  smaller than a given error  $\delta F$ , allowing efficient computations of the DF with sufficient accuracy.

The resulting  $\chi_N^2$  for each model are also displayed in Fig. 1. Evidently,  $N = 10$  components are more than sufficient to obtain very accurate dynamical models. As an example, Fig. 2 shows the 10 individual components of the QP-model with  $\beta_\infty = 0.4$ . Although this fit has the highest  $\chi_{10}^2$  of our set, its total density is a very close approximation to the given data over the entire range in radius.

### 4.2. The moments

Fig. 3 displays several moments for our six models, with 10 components. The top row shows the density  $\rho(r)$ , the pseudo phase-space density  $Q_r(r)$ , and the  $\beta - \gamma$  relation. Below each graph, we calculated the residual errors between the QP-fits

TABLE 1  
COMPONENTS OF THE SIX QP-MODELS.

	1	2	3	4	5	6	7	8	9	10
	$\beta_0 = 0.0,$	$\beta_\infty = 0.0,$	$s = 4/9,$	$\delta = 2/9$	$p_i = 3.4\bar{4}, 4, 5, 7.5, 10$			$q_i = -0.\bar{6}3, -0.5, -0.4, -0.3, -0.15, 0$		
$a_{10,i}$	0.2047	-0.0380	-0.5411	1.6652	0.0414	-3.8806	0.1312	2.5207	-0.2684	1.1652
$\rho_{0i}$	0.0053	1.9783	0.0009	2.5540	0.4890	3.0677	0.0384	3.6728	6.1920	0.0008
$p_i$	4.0000	10.0000	3.4444	10.0000	7.5000	10.0000	5.0000	10.0000	10.0000	3.4444
$q_i$	-0.6364	-0.6364	0.0000	-0.5000	-0.6364	-0.4000	-0.6364	-0.3000	0.0000	-0.6364
$\chi^2_N$	$0.44 \cdot 10^0$	$0.17 \cdot 10^0$	$0.67 \cdot 10^{-1}$	$0.33 \cdot 10^{-1}$	$0.24 \cdot 10^{-2}$	$0.17 \cdot 10^{-2}$	$0.53 \cdot 10^{-4}$	$0.36 \cdot 10^{-4}$	$0.48 \cdot 10^{-5}$	$0.82 \cdot 10^{-7}$
	$\beta_0 = 0.0,$	$\beta_\infty = 0.2,$	$s = 4/9,$	$\delta = 2/9$	$p_i = 3.0\bar{4}, 4, 5, 7.5, 10$			$q_i = -0.\bar{6}3, -0.5, -0.4, -0.3, -0.15, 0$		
$a_{10,i}$	-0.1534	15.5467	-0.0006	0.4549	-0.2707	74.2329	-88.6417	0.5880	-0.7724	0.0165
$\rho_{0i}$	0.0238	0.0017	3.4087	4.4609	11.3269	0.0014	0.0015	8.6356	5.4102	0.9797
$p_i$	4.0000	3.0444	10.0000	10.0000	10.0000	3.0444	3.0444	10.0000	10.0000	7.5000
$q_i$	-0.6364	0.0000	-0.6364	-0.5000	0.0000	-0.6364	-0.5000	-0.1500	-0.4000	-0.6364
$\chi^2_N$	$0.48 \cdot 10^0$	$0.27 \cdot 10^0$	$0.43 \cdot 10^{-1}$	$0.93 \cdot 10^{-2}$	$0.13 \cdot 10^{-2}$	$0.88 \cdot 10^{-3}$	$0.10 \cdot 10^{-4}$	$0.95 \cdot 10^{-5}$	$0.48 \cdot 10^{-5}$	$0.32 \cdot 10^{-7}$
	$\beta_0 = 0.0,$	$\beta_\infty = 0.4,$	$s = 4/9,$	$\delta = 2/9$	$p_i = 2.6\bar{4}, 4, 5, 8, 12$			$q_i = -0.\bar{6}3, -0.5, -0.4, -0.3, -0.15, 0$		
$a_{10,i}$	8.2375	-1.4318	-0.0467	0.2297	2.2705	-0.0111	0.1299	10.3097	-0.3108	-18.3771
$\rho_{0i}$	0.0832	0.0032	10.9019	14.9246	0.0028	2.4301	23.3335	0.1015	18.6978	0.0934
$p_i$	4.0000	2.6444	12.0000	12.0000	2.6444	8.0000	12.0000	4.0000	12.0000	4.0000
$q_i$	-0.6364	0.0000	-0.6364	-0.5000	-0.6364	-0.6364	-0.3000	-0.4000	-0.4000	-0.5000
$\chi^2_N$	$0.48 \cdot 10^0$	$0.18 \cdot 10^0$	$0.28 \cdot 10^{-1}$	$0.93 \cdot 10^{-2}$	$0.42 \cdot 10^{-2}$	$0.14 \cdot 10^{-3}$	$0.36 \cdot 10^{-4}$	$0.13 \cdot 10^{-4}$	$0.68 \cdot 10^{-5}$	$0.24 \cdot 10^{-6}$
	$\beta_0 = 0.0,$	$\beta_\infty = 0.6,$	$s = 4/9,$	$\delta = 2/9$	$p_i = 2.2\bar{4}, 3.5, 5, 8, 12$			$q_i = -0.\bar{6}3, -0.5, -0.4, -0.3, -0.15, 0$		
$a_{10,i}$	0.3552	2.0738	-0.0094	0.0086	16.3498	-17.4861	0.0731	-0.3019	-0.2109	0.1477
$\rho_{0i}$	0.1222	0.0063	16.7922	23.2672	0.0053	0.0055	4.3156	0.1372	8.0592	10.5109
$p_i$	3.5000	2.2444	12.0000	12.0000	2.2444	2.2444	8.0000	3.5000	8.0000	8.0000
$q_i$	-0.6364	0.0000	-0.6364	-0.5000	-0.6364	-0.5000	-0.6364	-0.5000	-0.3000	-0.1500
$\chi^2_N$	$0.44 \cdot 10^0$	$0.15 \cdot 10^0$	$0.18 \cdot 10^{-1}$	$0.67 \cdot 10^{-2}$	$0.31 \cdot 10^{-2}$	$0.16 \cdot 10^{-4}$	$0.13 \cdot 10^{-4}$	$0.10 \cdot 10^{-4}$	$0.17 \cdot 10^{-5}$	$0.20 \cdot 10^{-6}$
	$\beta_0 = 0.0,$	$\beta_\infty = 0.8,$	$s = 4/9,$	$\delta = 2/9$	$p_i = 1.8\bar{4}, 3, 5, 8, 12$			$q_i = -0.\bar{6}3, -0.5, -0.4, -0.3, -0.15, 0$		
$a_{10,i}$	-0.0321	-6.1421	0.0008	-0.0013	24.5830	-100.0000	-0.0163	-0.0926	40.5233	42.1774
$\rho_{0i}$	0.1791	0.0121	25.3820	35.5933	0.0101	0.0109	2.3877	0.2367	0.0105	0.0116
$p_i$	3.0000	1.8444	12.0000	12.0000	1.8444	1.8444	5.0000	3.0000	1.8444	1.8444
$q_i$	-0.6364	0.0000	-0.6364	-0.5000	-0.6364	-0.4000	-0.3000	-0.3000	-0.5000	-0.1500
$\chi^2_N$	$0.40 \cdot 10^0$	$0.11 \cdot 10^0$	$0.11 \cdot 10^{-1}$	$0.46 \cdot 10^{-2}$	$0.22 \cdot 10^{-2}$	$0.66 \cdot 10^{-5}$	$0.26 \cdot 10^{-5}$	$0.13 \cdot 10^{-5}$	$0.47 \cdot 10^{-6}$	$0.24 \cdot 10^{-6}$
	$\beta_0 = 0.0,$	$\beta_\infty = 1.0,$	$s = 4/9,$	$\delta = 2/9$	$p_i = 1.4\bar{4}, 3, 5, 8, 12$			$q_i = -0.\bar{6}3, -0.5, -0.4, -0.3, -0.15, 0$		
$a_{10,i}$	-5.2047	0.1086	62.6962	40.1800	-0.0002	0.0003	-96.6969	-0.1234	0.0273	0.0128
$\rho_{0i}$	0.0192	2.9967	0.0201	0.0213	37.6938	44.2497	0.0207	3.7237	7.8118	0.8543
$p_i$	1.4444	5.0000	1.4444	1.4444	12.0000	8.0000	1.4444	5.0000	5.0000	3.0000
$q_i$	-0.6364	-0.6364	-0.5000	-0.3000	-0.6364	0.0000	-0.4000	-0.5000	0.0000	-0.1500
$\chi^2_N$	$0.35 \cdot 10^0$	$0.36 \cdot 10^{-1}$	$0.10 \cdot 10^{-1}$	$0.24 \cdot 10^{-3}$	$0.41 \cdot 10^{-4}$	$0.16 \cdot 10^{-4}$	$0.13 \cdot 10^{-4}$	$0.45 \cdot 10^{-6}$	$0.89 \cdot 10^{-7}$	$0.22 \cdot 10^{-8}$

NOTE. — Our six models are determined by the anisotropy parameters  $\beta_0 = 0$  and  $\beta_\infty$ . With the QP-algorithm, we built linear combinations up to 10 components, each characterized by  $s$ ,  $\delta$ ,  $p_i$ ,  $q_i$  and  $\rho_{0i}$ . The parameters  $s$  and  $\delta$  are the same for each component, while  $p_i$  and  $q_i$  are selected from a library of 30 components. The five  $p_i$  values and six  $q_i$  values in each library are given in the headers. Every  $N$ th column lists the value  $\chi^2_N$  of the best fit with the first  $N$  components. The coefficients are given for the final fit with 10 components, i.e.  $a_{10,i}$ .

and the theoretical curves, i.e. for each profile  $f(r)$  we have

$$\Delta f(r) = \frac{f_{\text{obs}}(r) - f_{\text{qp}}(r)}{f_{\text{obs}}(r)}. \quad (58)$$

As can be seen, the relative errors on the densities are less than  $10^{-3}$  along 7 orders of magnitude in radius, and the exact asymptotic slopes of the models ensure excellent fits even beyond this range. The power-law trend of  $Q_r(r)$  and the  $\beta - \gamma$  relations are also reproduced very accurately with errors  $\sim 10^{-3}$ . Note that the small offset between the pseudo phase-space density profiles for the different models is due to the dependence of  $\sigma_r(r)$  on  $\beta_\infty$ .

In the central row, we display the velocity dispersion pro-

files  $\sigma_r(r)$ ,  $\sigma_\theta(r)$ , and the anisotropies  $\beta(r)$ . It is striking that, while the dispersion data were not used in the fit, the deviations of these moments from the theoretical values are even smaller, less than  $5 \cdot 10^{-4}$ . Evidently, since the models have the anisotropies (22) by construction, the  $\beta(r)$  profiles are exact, without errors. Note also that all tangential velocity dispersion profiles  $\sigma_\theta(r)$  intersect at a common radius  $r = r_s (9/11)^{1/\eta}$ .

While the density and dispersions are defined by the Dehnen-McLaughlin halos, the higher-order moments are determined by the QP-models. The fourth-order moments (see Appendix A) allow us to derive the radial and tangential kur-

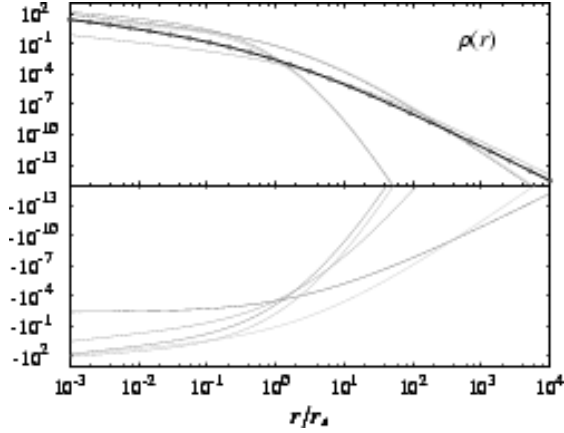


FIG. 2.— The 10 individual components of the fitted density for the QP-model with  $\beta_0 = 0$  and  $\beta_\infty = 0.4$ . Their sum is the QP-density (black thick curve), fitting the 25 data points (dots).

tosis,

$$\kappa_r(r) = \frac{\langle v_r^4 \rangle}{\sigma_r^4}(r) - 3, \quad (59)$$

$$\kappa_\theta(r) = \frac{\langle v_\theta^4 \rangle}{\sigma_\theta^4}(r) - 3, \quad (60)$$

and the fourth-order anisotropy

$$\beta_4(r) = 1 - \frac{\langle v_\theta^4 \rangle}{\langle v_r^4 \rangle}(r). \quad (61)$$

Interestingly, as a result of the separable form of the augmented densities, we find that the  $\beta_4(r)$  profiles are only a function of the  $\beta(r)$ ,

$$\beta_4(r) = \frac{1}{2}\beta(r)(3 - \beta(r)) + \frac{1}{2\beta_\delta}(\beta_0 - \beta(r))(\beta_\infty - \beta(r)). \quad (62)$$

These profiles are shown in the bottom row of Fig. 3. The kurtosis values describe the non-Gaussianity of the velocity distributions at a certain radius. Our radial kurtosis values are very large in the center, which indicates that the  $v_r$ -distributions are very peaked (leptokurtic) at small radii. The  $\kappa_r(r)$  curves decrease rapidly as a function of radius: they reach zero at radii between 0.26-0.36 and become negative at larger radii, leading to flat-topped (platykurtic) radial velocity distributions. This behavior is in accordance with  $N$ -body simulations (Kazantzidis et al. 2004; Wojtak et al. 2005). Clearly, the value of  $\beta_\infty$  has little influence on the radial kurtosis, as in the case of  $Q_r(r)$ . In contrast, the tangential kurtosis  $\kappa_\theta(r)$  curves do depend significantly on  $\beta_\infty$ . All  $v_\theta$ -distributions are highly peaked at small radii. For  $\beta_\infty < 0.4$  the tangential kurtosis decreases to slightly negative values, i.e. at larger radii the tangential velocity distributions become slightly flat-topped. Models with  $\beta_\infty \approx 0.4$  have nearly Gaussian  $v_\theta$ -distributions for  $r > r_s$ . If  $\beta_\infty > 0.4$ , the  $\kappa_\theta(r)$  profiles reach a minimum value and increase again for larger radii.

#### 4.3. The distribution functions

The six top panels of Fig. 4 show the distribution functions  $F(E, L)$  of our radially anisotropic systems with  $\beta_0 = 0$  and  $\beta_\infty = 0, \dots, 1$ , expressed as logarithmic isoproability contours and a logarithmic color gradient in the integral space, with  $L$  scaled to  $L_c(E)$ , denoting the angular momentum of a circular orbit with energy  $E$ . All models are clearly physical,

i.e. the DFs are non-negative everywhere. This means that the Dehnen-McLaughlin Jeans models can actually be realized by full dynamical models. Moreover, contrary to the Osipkov-Merritt models, these functions fill the entire integral space. In the isotropic case, the contours are horizontal (no dependence on angular momentum), and their orientation alters gradually with increasing  $\beta_\infty$  in an intuitive way, as orbits with high eccentricities (i.e. low angular momentum) become more abundant.

The DFs describe the probability distributions of particles in phase space, but not in the integral space. It is more physically meaningful to consider the true orbital distributions

$$N(E, L/L_c(E)) = F(E, L)g(E, L)L_c(E), \quad (63)$$

with the so-called "density of states" function

$$g(E, L) = 16\pi^2 L \int_{r_-}^{r_+} \frac{dr}{\sqrt{2(\psi(r) - E) - L^2/r^2}}, \quad (64)$$

where  $r_-$  and  $r_+$  are the pericenter and apocenter of an orbit with energy  $E$  and angular momentum  $L$ . In other words, the functions  $N(E, L/L_c(E))$  express the likelihood of an orbit with energy  $E$  and scaled angular momentum  $L/L_c(E)$ .

The results are displayed in the bottom panels of Fig. 4 as logarithmic isoproability contours and a logarithmic color gradient in the integral space. For high binding energies, all orbital distributions contain increasing probabilities toward circular orbits (high angular momentum). For low binding energies, i.e. at large radii, the abundance of orbits with low angular momentum gradually increases from the isotropic case to models with high values of  $\beta_\infty$ .

#### 4.4. The marginal distributions

We conclude the discussion of our Dehnen-McLaughlin DFs with an analysis of the marginal distributions. The differential energy and angular momentum distributions are the integrals of the orbital distributions,

$$N(E) = \int_0^{L_c(E)} N(E, L) dL, \quad (65)$$

$$N(L) = \int_0^{E_c(L)} N(E, L) dE, \quad (66)$$

with

$$N(E, L) = \frac{1}{L_c(E)} N(E, L/L_c(E)). \quad (67)$$

These curves are displayed in Fig. 5. The differential energy distributions are all monotonously decreasing functions of  $E$ . It is striking that these profiles are almost identical, regardless of the anisotropy  $\beta_\infty$ . This result reinforces previous dynamical studies (Binney 1982), and suggests that  $\rho(r)$ ,  $Q_r(r)$  and  $\kappa_r(r)$  are linked to a universal differential energy distribution, independent of  $\beta_\infty$ , caused by the same physical processes.

In contrast, the angular momentum distributions depend on  $\beta_\infty$ , most notably for high radial anisotropies. For increasing values of  $\beta_\infty$ , the fraction of orbits with low angular momentum increases. Bullock et al. (2001) proposed a universal form for the integrated angular momentum distribution in dark matter halos  $M(L)$ . Alternatively, Sharma & Steinmetz (2005) found a differential distribution

$$N_{ss}(L) = \frac{1}{L_d^a \Gamma(a)} L^{a-1} e^{-L/L_d}. \quad (68)$$

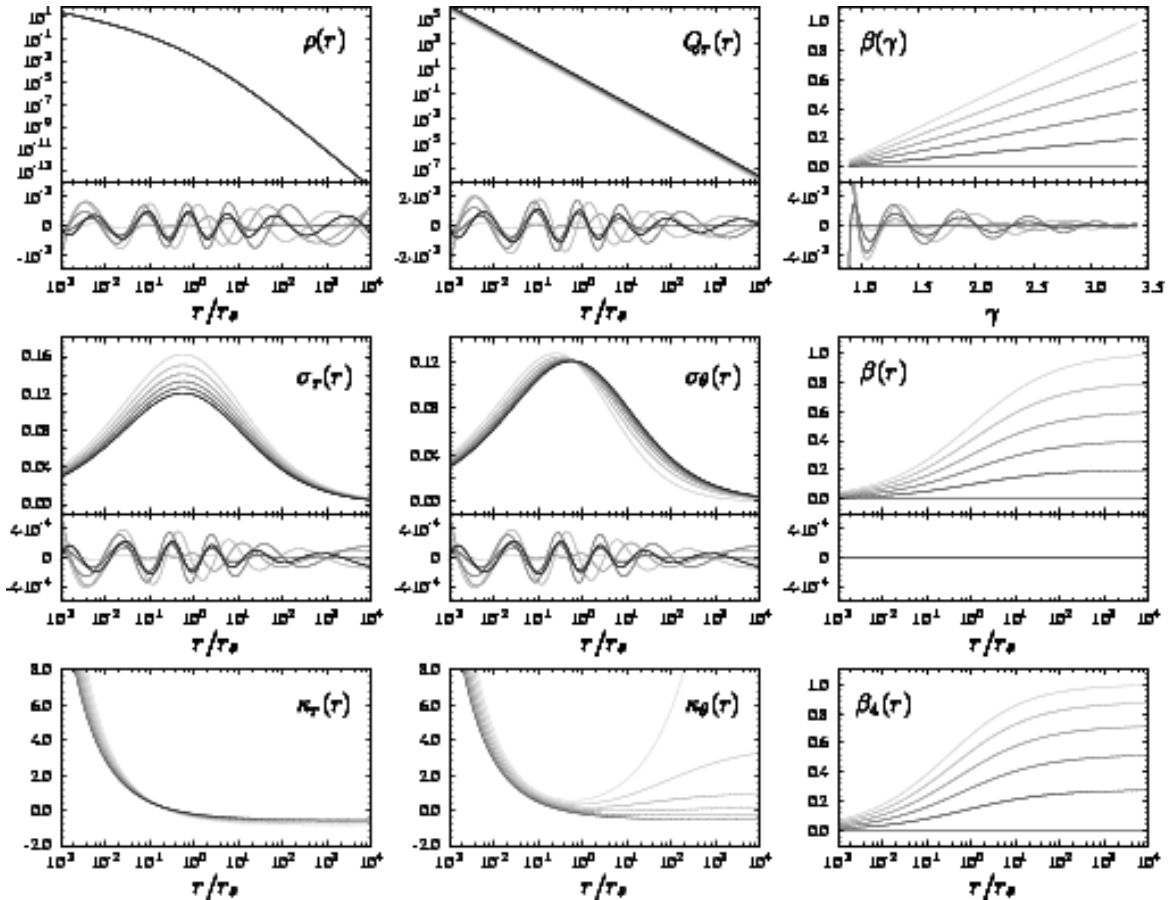


FIG. 3.— The most important moments for our set of representative models with 10 components. Top row: the density  $\rho(r)$ , the pseudo phase-space density  $Q_r(r)$  and the  $\beta-\gamma$  relation. Below each graph, the relative errors with respect to the theoretical profiles is shown. Middle row: the radial velocity dispersion  $\sigma_r(r)$ , the tangential velocity dispersion  $\sigma_\theta(r)$ , and the anisotropy  $\beta(r)$ , also with the relative errors. Bottom row: the radial kurtosis  $\kappa_r(r)$ , the tangential kurtosis  $\kappa_\theta(r)$ , and fourth-order anisotropy  $\beta_4(r)$ . The models and grayscaling are the same as in Fig. 1.

Our models indicate a similar profile, with  $a > 0.9$ , although the functions (68) fall steeper than ours as  $L$  increases.

## 5. CONCLUSIONS

In this paper we presented a set of anisotropic distribution functions  $F(E, L)$  for the Dehnen-McLaughlin Jeans models. We constructed these DFs as a linear combination of base functions, which we fitted to the halo density by means of a quadratic programming algorithm. The base functions were specifically designed for this task, derived from a separable augmented density that generates exactly the general four-parameter velocity anisotropy profiles (5). We demonstrated that the resulting fits are very accurate, from the center to large radii, far beyond the range of  $N$ -body simulations.

This method has several advantages. The DFs can be written as a sum of a double series, without numerical integrations or inversions. Consequently, the DFs and all subsequent moments can be computed with high accuracy. Moreover, the advanced form of the base functions makes the QP-fitting very fast, requiring only a small number of library components.

In this manner, we have constructed a family of dynamical models that incorporate the observed features in  $N$ -body simulations. We summarize their properties:

1. The models a priori have the universal properties encountered in  $N$ -body studies of dark matter halos, which formed the building bricks of the Jeans models by Dehnen & McLaughlin (2005): they generate a universal density profile, a power-law pseudo phase-space

density  $Q_r(r)$ , four-parameter velocity anisotropy profiles with arbitrary values of  $\beta_0$  and  $\beta_\infty$ , and a linear  $\beta-\gamma$  relation. In particular, we analyzed six models that are isotropic in the center and radially anisotropic at large radii.

2. The DFs are physical, i.e. they are non-negative over the entire phase space. This means that the Dehnen-McLaughlin Jeans models can actually be realized by self-consistent dynamical systems. In addition, the DFs are continuous and smooth functions and, contrary to the popular Osipkov-Merritt models, they fill the entire accessible phase space.
3. The energy distributions are monotonously decreasing functions, and like the radial kurtosis profiles, these functions are nearly independent of  $\beta_\infty$ . This suggests that  $\rho(r)$ ,  $Q_r(r)$ ,  $\kappa_r(r)$ , and  $N(E)$  have a universal form, caused by the same physical processes.

In addition, we have also been able to generate dynamical models with a non-linear  $\beta-\gamma$  relation, i.e.  $\delta \neq \eta/2$  and  $r_a \neq r_s$ , albeit with higher  $\chi_N^2$  values. From these successful results for the Dehnen-McLaughlin halos, we expect equally adequate fits for other Zhao models, such as the NFW halos. Other profiles, such as the Sérsic-type densities, might require a modified family of base functions. Such a systematic study could unravel more hitherto hidden properties of dark matter halos, and the various connections between these characteristics.

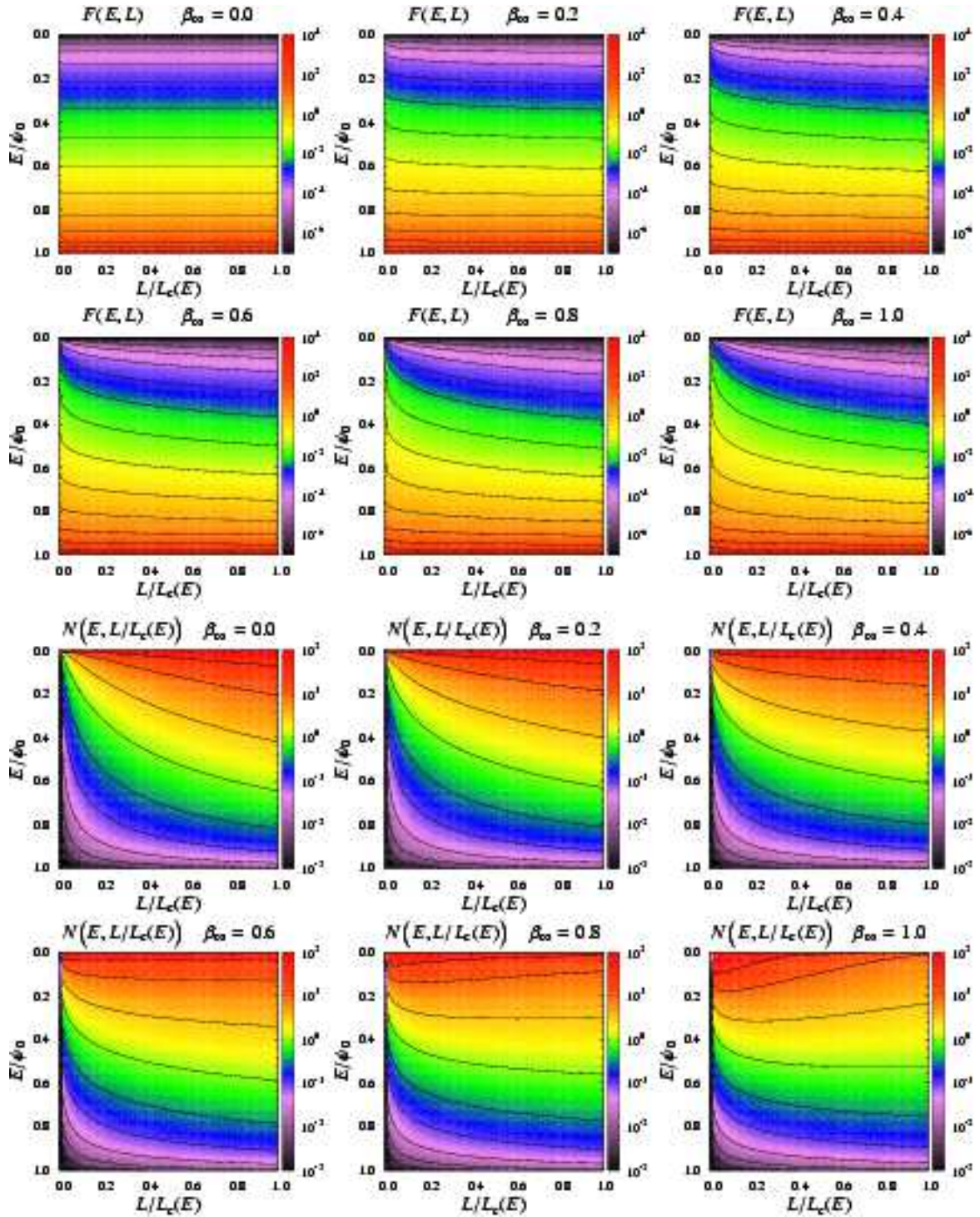


FIG. 4.— The phase-space distribution functions for our set of models with 10 components. The six top panels show  $F(E, L)$  as isoprobability contours in the integral space. The energy is scaled to the central potential and the angular momentum is scaled to the angular momentum  $L_c(E)$  of a circular orbit with energy  $E$ . The contour levels and the coloring are scaled logarithmically. The six bottom panels show the orbital distribution functions  $N(E, L/L_c(E))$  for the same models.

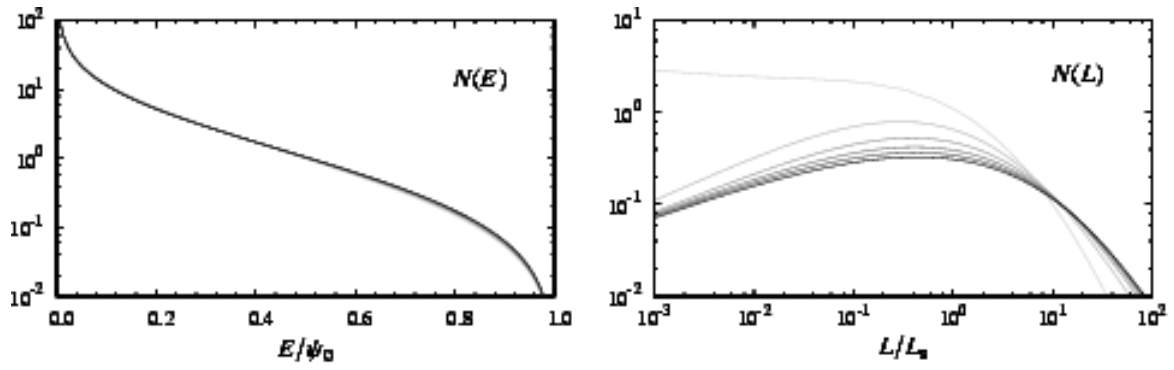


FIG. 5.— The energy and angular momentum distributions of the six QP-models with 10 components. The angular momenta are scaled to the values  $L_s$  of a circular orbit with radius  $r_s$ . The models and grayscaleing are the same as in Fig. 1.

Our set of dynamical models is not only useful for a purely theoretical analysis. The DFs can also serve to generate initial conditions with Monte Carlo simulators (e.g. Kazantzidis et al. 2004; Buyle et al. 2007b) to investigate the physical processes within these equilibrium models by means of controlled numerical  $N$ -body simulations. Finally, our al-

gorithm and base functions can be used in other dynamical studies, using different data moments than the density. This could lead to a significant improvement in the dynamical modeling of observed stellar systems, such as clusters of galaxies.

#### APPENDIX

##### DERIVATION OF THE AUGMENTED MOMENTS

In a spherical dynamical model, the anisotropic velocity moments of the DF are

$$\mu_{2n,2m}(r) = 2\pi M_{\text{tot}} \int_{-\infty}^{+\infty} dv_r \int_0^{+\infty} F(E, L) v_r^{2n} v_T^{2m+1} dv_T. \quad (\text{A1})$$

Using the augmented density formalism, these moments can be calculated as  $\mu_{2n,2m}(r) = \tilde{\mu}_{2n,2m}(\psi(r), r)$ , with

$$\tilde{\mu}_{2n,2m}(\psi, r) = \frac{2^{m+n}}{\sqrt{\pi}} \frac{\Gamma(n + \frac{1}{2})}{\Gamma(m+n)} \int_0^\psi (\psi - \psi')^{m+n-1} D_{r^2}^m [r^{2m} \tilde{\rho}(\psi', r)] d\psi', \quad (\text{A2})$$

where  $D_x^m$  denotes the  $m$ th differentiation with respect to  $x$ . Applying this to our base functions (44), we obtain for the augmented second-order moments

$$\tilde{\mu}_{20,i}(\psi, r) = \frac{\rho_{0i} \psi_0}{s_i} \left(\frac{r}{r_a}\right)^{-2\beta_0} \left(1 + \frac{r^{2\delta}}{r_a^{2\delta}}\right)^{\beta_\delta} B_y \left(\frac{1+p_i}{s_i}, 1+q_i\right), \quad (\text{A3})$$

with  $y = (\psi/\psi_0)^{s_i}$ , and

$$\tilde{\mu}_{02,i}(\psi, r) = 2(1 - \beta(r)) \tilde{\mu}_{20,i}(\psi, r). \quad (\text{A4})$$

The augmented fourth-order moments have the form

$$\tilde{\mu}_{40,i}(\psi, r) = \frac{3\rho_{0i} \psi_0^2}{s_i} \left(\frac{r}{r_a}\right)^{-2\beta_0} \left(1 + \frac{r^{2\delta}}{r_a^{2\delta}}\right)^{\beta_\delta} \left[ \frac{\psi}{\psi_0} B_y \left(\frac{1+p_i}{s_i}, 1+q_i\right) - B_y \left(\frac{2+p_i}{s_i}, 1+q_i\right) \right], \quad (\text{A5})$$

$$\tilde{\mu}_{22,i}(\psi, r) = 2(1 - \beta(r)) \tilde{\mu}_{40,i}(\psi, r), \quad (\text{A6})$$

$$\tilde{\mu}_{04,i}(\psi, r) = \frac{2}{3} \left[ (1 - \beta(r))(2 - \beta(r)) - \frac{1}{\beta_\delta} (\beta_0 - \beta(r)) (\beta_\infty - \beta(r)) \right] \tilde{\mu}_{40,i}(\psi, r). \quad (\text{A7})$$

The true velocity moments are connected with the anisotropic velocity moments through the relation

$$\tilde{\mu}_{2l,2m,2n}(\psi, r) = \frac{1}{\pi} B \left(m + \frac{1}{2}, n + \frac{1}{2}\right) \tilde{\mu}_{2l,2(m+n)}(\psi, r), \quad (\text{A8})$$

so that

$$\rho \sigma_r^2(r) = \mu_{200}(r) = \sum_{i=1}^N a_{N,i} \tilde{\mu}_{20,i}(\psi(r), r), \quad (\text{A9})$$

$$\rho \sigma_\theta^2(r) = \mu_{020}(r) = \frac{1}{2} \sum_{i=1}^N a_{N,i} \tilde{\mu}_{02,i}(\psi(r), r), \quad (\text{A10})$$

$$\rho \langle v_r^4 \rangle(r) = \mu_{400}(r) = \sum_{i=1}^N a_{N,i} \tilde{\mu}_{40,i}(\psi(r), r), \quad (\text{A11})$$

$$\rho \langle v_\theta^4 \rangle(r) = \mu_{040}(r) = \frac{3}{4} \sum_{i=1}^N a_{N,i} \tilde{\mu}_{04,i}(\psi(r), r). \quad (\text{A12})$$

Finally, the fourth-order anisotropy profile can be derived by combining eqs. (A7), (A11) and (A12),

$$\beta_4(r) = 1 - \frac{\langle v_\theta^4 \rangle}{\langle v_r^4 \rangle}(r) = \frac{1}{2} \beta(r) (3 - \beta(r)) + \frac{1}{2\beta_\delta} (\beta_0 - \beta(r)) (\beta_\infty - \beta(r)). \quad (\text{A13})$$

#### REFERENCES

- Baes, M. & Dejonghe, H. 2002, *A&A*, 393, 485  
Baes, M. & Van Hese, E. 2007, *A&A*, 471, 419 (Paper I)  
Binney, J. 1982, *MNRAS*, 200, 951  
Bullock, J. S., Dekel, A., Kolatt, T. S., et al. 2001, *ApJ*, 555, 240  
Buyle, P., Hunter, C., & Dejonghe, H. 2007a, *MNRAS*, 375, 773  
Buyle, P., Van Hese, E., De Rijcke, S., & Dejonghe, H. 2007b, *MNRAS*, 375, 1157  
Carlberg, R. G., Yee, H. K. C., Ellingson, E., et al. 1997, *ApJ*, 485, L13+  
Crone, M. M., Evrard, A. E., & Richstone, D. O. 1994, *ApJ*, 434, 402  
Dehnen, W. & McLaughlin, D. E. 2005, *MNRAS*, 363, 1057  
Dejonghe, H. 1986, *Phys. Rep.*, 133, 217  
Dejonghe, H. 1987, *MNRAS*, 224, 13  
Dejonghe, H. 1989, *ApJ*, 343, 113  
Diemand, J., Zemp, M., Moore, B., Stadel, J., & Carollo, C. M. 2005, *MNRAS*, 364, 665  
Dubinski, J. & Carlberg, R. G. 1991, *ApJ*, 378, 496  
Fox, C. 1961, *Trans. Amer. Math. Soc.*, 98, 395  
Fricke, W. 1952, *Astronomische Nachrichten*, 280, 193  
Fukushige, T. & Makino, J. 1997, *ApJ*, 477, L9+  
Gerhard, O., Jeske, G., Saglia, R. P., & Bender, R. 1998, *MNRAS*, 295, 197  
Hansen, S. H. & Moore, B. 2006, *New Astronomy*, 11, 333  
Hernquist, L. 1990, *ApJ*, 356, 359  
Hernquist, L. 1993, *ApJS*, 86, 389  
Jing, Y. P. & Suto, Y. 2000, *ApJ*, 529, L69  
Kazantzidis, S., Magorrian, J., & Moore, B. 2004, *ApJ*, 601, 37  
Kuijken, K., & Merrifield, M. R. 1993, *MNRAS*, 264, 712  
Łokas, E. L. & Mamon, G. A. 2001, *MNRAS*, 321, 155  
Mamon, G. A. & Łokas, E. L. 2005, *MNRAS*, 363, 705  
Merrifield, M. R., & Kuijken, K. 1994, *ApJ*, 432, 575  
Merritt, D. 1985, *AJ*, 90, 1027  
Merritt, D., Graham, A. W., Moore, B., Diemand, J., & Terzić, B. 2006, *AJ*, 132, 2685  
Merritt, D., Navarro, J. F., Ludlow, A., & Jenkins, A. 2005, *ApJ*, 624, L85  
Moore, B., Governato, F., Quinn, T., Stadel, J., & Lake, G. 1998, *ApJ*, 499, L5+  
Moore, B., Quinn, T., Governato, F., Stadel, J., & Lake, G. 1999, *MNRAS*, 310, 1147  
Navarro, J. F., Frenk, C. S., & White, S. D. M. 1996, *ApJ*, 462, 563  
Navarro, J. F., Frenk, C. S., & White, S. D. M. 1997, *ApJ*, 490, 493  
Navarro, J. F., Hayashi, E., Power, C., et al. 2004, *MNRAS*, 349, 1039  
Osipkov, L. P. 1979, *Pis ma Astronomicheskii Zhurnal*, 5, 77  
Rasia, E., Tormen, G., & Moscardini, L. 2004, *MNRAS*, 351, 237  
Sharma, S. & Steinmetz, M. 2005, *ApJ*, 628, 21  
Taylor, J. E. & Navarro, J. F. 2001, *ApJ*, 563, 483  
Veltmann, U. I. K. 1979, *AZh*, 56, 976  
Widrow, L. M. 2000, *ApJS*, 131, 39  
Wojtak, R., Łokas, E. L., Gottlöber, S., & Mamon, G. A. 2005, *MNRAS*, 361, L1  
Wojtak, R., Łokas, E. L., Mamon, G. A., Gottlöber, S., Klypin, A., & Hoffman, Y. 2008, *MNRAS*, 719  
Zhao, H. 1996, *MNRAS*, 278, 488